Sensors & Actuators: B. Chemical 347 (2021) 130589

Contents lists available at ScienceDirect

Sensors and Actuators: B. Chemical

journal homepage: www.elsevier.com/locate/snb

Acoustically-actuated bubble-powered rotational micro-propellers[☆]

Sumit Mohanty [a,*], Jiena Zhang [b], Jeffrey M. McNeill [c], Thom Kuenen [a], Frederic P. Linde [a], Jeroen Rouwkema [b], Sarthak Misra [a,d,1]

[a] Surgical Robotics Laboratory, Department of Biomechanical Engineering, University of Twente, 7522 NB Enschede, The Netherlands
[b] Vascularization Lab, Department of Biomechanical Engineering, University of Twente, 7522 NB Enschede, The Netherlands
[c] Department of Chemistry, University of Pennsylvania, Philadelphia, Pennsylvania 19104, United States
[d] Surgical Robotics Laboratory, Department of Biomedical Engineering, University of Groningen and University Medical Center Groningen, 9713 AV Groningen, The Netherlands

ARTICLE INFO

Keywords:
Microrobotics
Acoustic streaming
Acoustofluidics
Bubble-powered motors
Self-propulsion
Minimally-invasive surgeries
Ultrasound

ABSTRACT

Bubble-powered acoustic microsystems span a plethora of applications that range from lab-on-chip diagnostic platforms to targeted interventions as microrobots. Numerous studies strategize this bubble-powered mechanism to generate autonomous self-propulsion of microrobots in response to high frequency sound waves. Herein, we present two micro-propeller designs which contain an axis-symmetric distribution of entrapped bubbles that vibrate to induce fast rotational motion. Our micro-propellers are synthesized using 3D Direct Laser Writing and chemically-functionalized to selectively trap air bubbles at their micro-cavities which function as propulsion units. These rotational acoustic micro-propellers offer a dual advantage of being used as mobile microfluidic mixers, and as autonomous microrobots for targeted manipulation. With regards to targeted manipulation, we demonstrate magneto-acoustic actuation of our first propeller design that can be steered to a desired location to perform rotational motion. Furthermore, our second propeller design comprises of a helical arrangement of bubble-filled cavities which makes it suitable for spatial micro-mixing. Our acoustic propellers can reach speeds of up to 400 RPM (rotations per minute) without requiring any direct contact with a vibrating substrate in contrast to the state-of-the-art rotary acoustic microsystems.

1. Introduction

A myriad of biomedical technologies have evolved from contactless micromanipulation methods powered by external sources such as magnetism [1], optics [2], acoustics [3] and chemical reactions [4]. These methods encompass both microrobotic applications such as targeted therapy [5], and microfluidics diagnostic platforms [6]. Among these methods, magnetic and acoustic means of remote actuation rose to prominence due to their complimentary nature to existing medical imaging technologies like magnetic resonance (MR) [7] and ultrasound (US) systems [8]. Despite the popularity of magnetically-actuated microsystems, it is challenging to fabricate such systems with sufficient magnetic content at micro-nano scale which limits the propulsive forces offered by their sub-components [9]. Additionally, some of these magnetic components either require bulky permanent magnets or electromagnets for actuation, or move with low speeds owing to bandwidth-limited electromagnetic systems i.e., <150 Hz [10,11]. These limitations have precipitated a shift towards acoustically-actuated microsystems as alternatives to other remote actuation techniques.

Owing to the biocompatibility of sound waves in *in-vivo* applications, and their wide available range of operating frequencies (100 Hz–1 GHz), various techniques of acoustic actuation have been explored [12–17]. These techniques encompass biological applications from tissue organization induced by standing waves [14,15] to targeted drug delivery [16,17]. High frequency acoustic fields have been capitalized in form of vibrating air bubbles [18,19] and sharp protrusions [20–22] to facilitate

☆ This work is supported by funds from The Netherlands Organization for Scientific Research (Innovational Research Incentives Scheme-VIDI: SAMURAI project #14855).

* Corresponding author.
E-mail addresses: s.mohanty@utwente.nl (S. Mohanty), j.zhang-6@utwente.nl (J. Zhang), jmm1125@sas.upenn.edu (J.M. McNeill), t.c.g.kuenen@student.utwente.nl (T. Kuenen), f.p.linde@student.utwente.nl (F.P. Linde), j.rouwkema@utwente.nl (J. Rouwkema), s.misra@utwente.nl, s.misra@umcg.nl (S. Misra).
URL: https://surgicalroboticslab.nl/ (S. Misra).
[1] Principal corresponding author.

https://doi.org/10.1016/j.snb.2021.130589
Received 27 May 2021; Received in revised form 14 July 2021; Accepted 6 August 2021
Available online 12 August 2021

movable components in microsystems such as propellers, gears and mixers. Particularly, microsystems with entrapped air bubbles have proven to be the most ubiquitous toolbox for acousto-fluidic platforms due to their ability to produce localized fluid currents under acoustic excitation [23]. Another example of acoustically-actuated tools are the bubble-powered micro-propellers. Such propellers hold the potential to remotely perform targeted operations under inaccessible *in-vivo* conditions beyond the reach of tethered surgical instruments. These propellers typically comprise of a one-sided entrapped bubble that vibrates to impart them a directional self-propulsion for such targeted applications [3,18,24–26]. However, these bubble-powered propellers consist of a single entrapped bubble where longevity of this bubble limits the lifetime of the propeller. Furthermore, many of these propellers depend on additional mechanisms for steering, such as acoustic radiation forces [24] or application of magnetic torques [18,27,25,26]. Besides these propellers, only a few designs exist that can rotate or steer themselves solely based on bubble-powered actuation [28,24,29]. Such limitations call for alternate approaches for design and operation of bubble-powered micro-propellers.

In recent years, the design and actuation strategy of many steerable acoustic micro-propellers have been inspired from the rotational motion of gears and mixers. These propellers often consist of an axis-symmetric distribution of acoustically-actuated components. Specifically, a series of multi-cavity propellers have evolved to contain equal and opposite pairs of bubble-entrapped cavities that facilitate multiple degrees of motion [29,28,30]. However, these propellers are milli-scale and can be acoustically-steered with slower rotational speeds i.e., <200 RPM [29,31]. Numerous microfluidics platforms also utilize gears with axis-symmetric protrusions or bubble-filled cavities that vibrate to achieve fast rotational speeds up to 1000 RPM [22,21,32–34]. A disadvantage with such gears is that their functionalities are confined to the microfluidic channels as the vibrational units are tethered to the respective channel substrates. This limitation affects the production costs and resuability of such microsystems. In addition, the synthesis of such specialized microfluidic gears requires sophisticated multi-step fabrication procedures. Such procedures often require more specialized equipment as compared to standard microchannel synthesis. Importantly, a majority of these microfluidic gears are tethered to their actuated substrates for their functionality [31,34,22,21,32,33]. This limitation presents an opportunity to redesign the bubble-powered propellers to reproduce the same rotational motion in an untethered fashion.

Herein, we introduce two micro-propellers which comprise of an axis-symmetric distribution of bubble-entrapped cavities that vibrate to produce rotational motion akin to a gear. Unlike the tethered gears, these propellers do not require any direct contact with a vibrating substrate for their actuation. We first present a simplistic gear-like propeller (Type I) with a 2-D axis-symmetric distribution of cavities (Fig. 1(a)). Here, the cavities produce propulsive forces at their open ends to produce a net force moment for rotation. Furthermore, we functionalize the Type I propellers with a magnetic layer to demonstrate their directional control under uniform magnetic fields. Contrary to other bubble-powered propellers, we devise a hybrid actuation strategy whereby Type I propellers rotate under acoustic fields and translate under combined magneto-acoustic fields. Thereon, we extend this design approach to present a Type II propeller (Fig. 1(b)) that comprises of a 3-D distribution of cavities arranged in a helical fashion around a propeller shaft. The Type II propellers offer a solution for spatial mixing as opposed to conventional 2-D design of micro-mixers and can reach comparably fast rotational speeds of up to 400 RPM. Thus, our bubble-powered micro-propellers provide an inexpensive solution to previously cited tethered microsystems as mobile micro-mixers that can be introduced and retrieved post-operation.

2. Material and methods

2.1. Experimental setup and fabrication details

Our micropropellers are composed of arrays of a cylindrical cavity enclosed with a spherical cap of the same diameter and thickness. These cavities form the building block of both Type I and Type II propellers which consist of a circular and helical distribution of four and thirteen cavities, respectively (Fig. 1(d) and 1 (e)). Both the Type I and II propellers are monolithic and are batch fabricated using Direct Laser Writing (DLW, Nanoscribe GmbH) with IP-Dip as the photoresist. Full description of the process parameters used for DLW printing and development is described in *SI, Appendix A*. Additionally, a batch of metallic Type I propeller is synthesized for magnetic steering experiments, where they are sputtered with a 240 nm layer of NiFe followed by a 50 nm layer of Au. For both these batches, the surface of the substrate containing the propellers is then activated in an oxygen plasma (50 W) for 40 s (Cute, Femto Science) prior to further processing. Thereon, the substrate is treated with 10 μL of trichlorosilane (PFOCTS, Merck) vapor at 55°C for 120 min in a closed chamber in order to make them

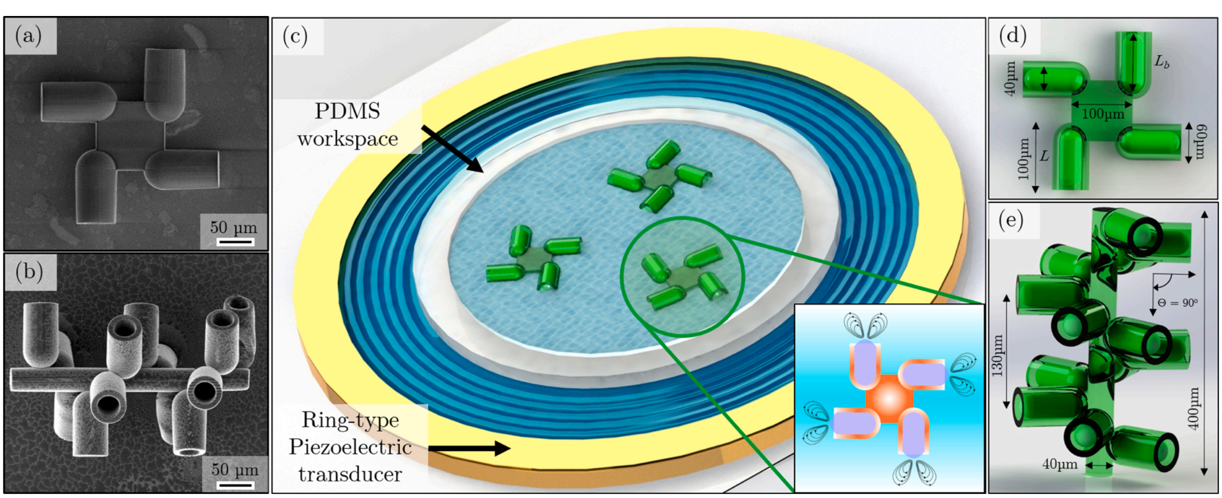

Fig. 1. Micrographs of (a) Type I propeller and (b) Type II propeller. (c) Acoustic actuation test-bed comprising of a ring-type piezoelctric transducer (Pz27, Meggitt) bonded to a glass substrate with a polydimethylsiloxane (PDMS) workspace on the opposite side. The test-bed shows Type I propellers immersed in phosphate-buffered saline (1x-PBS) solution mixed with polystyrene tracer particles (6μm diameter, Polysciences) where inset describes the streaming pattern around the bubbles upon acoustic excitation. (d–e) Schematic of Type I and II propellers with their respective dimensions, showing the cavity length (L), bubble length (L_b), and angular tilt of the cavity to Type II propeller shaft (θ).All the constituent cavities in both the propellers share the same dimension.

hydrophobic. This treatment ensures that the propellers readily trap bubbles once introduced in water. Following this step, the substrate is heated to 70°C for 15 min to get rid of the excessive layers of trichlorosilane. The heating step prevents the bubbles to slip out of the cavities. Lastly, the propellers are immersed in the acoustic actuation test-bed described in Fig. 1(c), where all the constituent cavities instantaneously trap bubbles. Acoustic actuation in our test-bed is enabled using a programmable signal generator (33510B, Keysight) connected to an amplifier. Additional details for image acquisition and electromagnetic setup for steering experiments are described in our prior work [9].

2.2. Working principle

2.2.1. Forces around the vibrating entrapped bubbles

A gaseous bubble immersed in water under an acoustic field experiences two kinds of forces. It experiences radiation forces due to the incoming sound waves, and the forces generated by oscillating fluid in the vicinity of vibrating bubble interface [12]. The latter is caused by counter-rotating fluid fluxes near the vibrating interface, known as acoustic streaming (Fig. 1(c) *inset*). Owing to the deformability of the bubbles, the radiation forces acting on them can be classified as primary and secondary Bjerknes forces. The primary Bjerknes forces act on the bubbles due to incoming sound waves from the source of excitation, and are typically an order of magnitude smaller than the streaming-induced forces and secondary Bjerknes forces (SBF) [3,18,24]. In case of our propeller cavities, vibration of bubbles generate a streaming-induced flow away from the cavities caused by the asymmetry of the entrapped bubbles. This net fluid flow that originates from the vibrating air-fluid interface in the entrapped bubbles manifests into a streaming-induced propulsive force (SPF) acting on each cavity. Further, owing to the symmetric distribution of cavities in both the propellers, they presume a position with all the cavities parallel to the substrate when acoustically-actuated (Movie S1). On the other hand, while SBF typically attracts bubbles to nearby surfaces, the presence of multiple entrapped bubbles in our propeller makes them buoyant when actuated. Moreover, since the SBF acts equally on all the constituent cavities when they are parallel to the substrate, there is no net unbalanced force or moment that imbalances the propellers from this position (Fig. 1(c)).

2.2.2. Computation of streaming patterns around bubble-powered propeller

We evaluate the streaming behavior around our propeller cavities using a computational model of a 2-D design of a Type I propeller. We adopted our simulation environment (COMSOL Multiphysics) based on the separation of time scales approach with a vibrating air-water interface [26]. First, we validate our model with the simulation of a double-lobed streaming pattern around a single isolated propeller cavity, as shown in Fig. 2(a-I). Next, we evaluate the streaming patterns around the Type I propeller as described in Fig. 2(a-II) and 2 (a-III). It is noteworthy that the direction of fluid flow around Type I propeller (*counter-clockwise*) is opposite to that of the distribution of propeller cavities (*clockwise*). Here, these arrows signify the reaction force exerted by a static propeller to the surrounding fluid suggestive of an equal and opposite direction of action force acting on the the propeller. We later find that this observation reciprocates in form of the propeller rotation as seen experimentally (Movie S1).

2.2.3. Resonant frequency of bubble-powered propeller

In order to identify the operating frequencies of our propeller, we investigate the acoustic resonance modes of its constituent bubbles. Traditionally, bubble-entrapped cavities have been modeled as a damped harmonic oscillator [19]. The resonant frequency (f_{res}) for such a bubble-entrapped cavity can be expressed as:

$$f_{res} = \frac{1}{2\pi}\left(\frac{\kappa P_{atm}}{\rho L_b (L - L_b)}\right)^{1/2} \quad (1)$$

where P_{atm}, κ and ρ represent the ambient pressure in the bubble, adiabatic index of air (<1.4) and density of the fluid (water), respectively. Given the length (L) of our constituent cavity as 100 μm, we calculated the resonant frequencies for a distribution of bubble lengths (L_b) (Fig. 2 (b-III)). As Eq. (1) in quadratic in L_b, the resonant frequency of the bubble is symmetric about $L_b = 50\,\mu$m. Thus, we explore a frequency range corresponding to $L_b = 50$–$90\,\mu$m, based on the expected performance in terms of bubbles entrapment i.e., $L_b > 50\mu$m. Theoretically, this distribution of $L_b = 50$–90μm corresponds to resonant frequencies in the range of 38–63 kHz. This range narrows down our investigation to the operating frequencies where both the transducer can deliver, and our propeller respond to acoustic power, respectively.

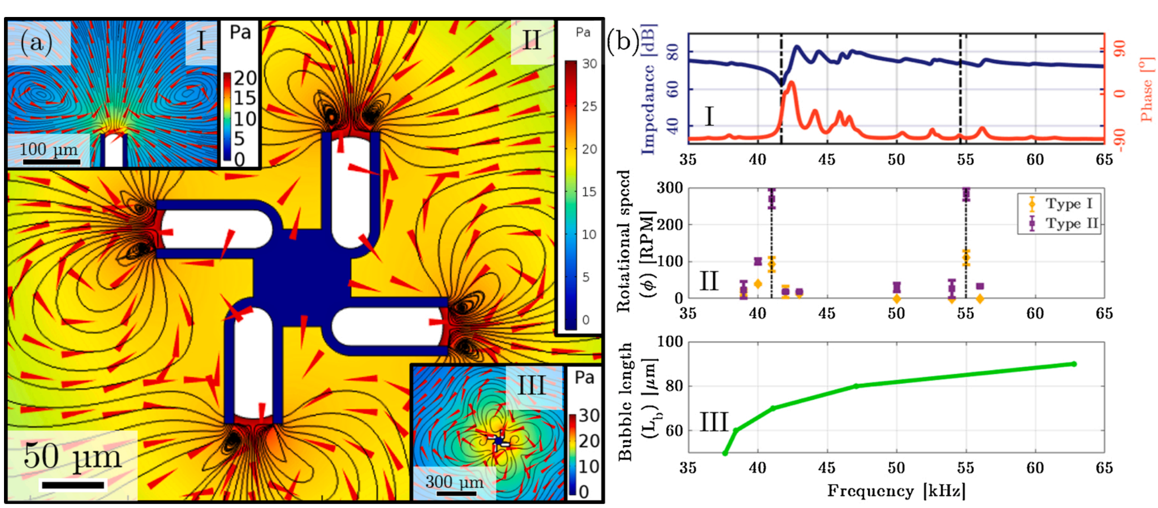

Fig. 2. (a) (I-III) Numerical computation of acoustic streaming around propeller geometry at an acoustic frequency of 50kHz. The red arrows represent particle velocity, black lines represent the streamlines and the color legend represents acoustic pressure in the respective graphs. (I) Double-loped streaming pattern around an isolated Type I/II propeller cavity. (II) Near field view: Streaming pattern around the constituent cavities of the Type I propeller interfere with each other owing to the close proximity of the neighboring cavities. (III) Far field view: Resultant net flow generated around Type I propeller shows a net flow in *counter-clockwise* direction. Additional details on the frequency-dependency of the streaming profile of Type I propellers is provided in *SI, Appendix B*. (b) (I-III) Frequency characterization of propellers and transducer. (I) Impedance characteristics of piezoelectric transducer (Pz27) (II) Frequency response of Type I and II propellers performed at a constant input voltage of $100V_{pk-pk}$. Here the rotational response of propellers is reported in rotations per minute (RPM). (III) Theoretical frequency for the propeller cavity as a function of bubble length (L_b).

3. Results and discussions

3.1. Frequency characterization of transducer and micro-propeller

We measure the resonant frequencies of the transducer in its impedance spectrum over previously mentioned concerned range using the approach described in our prior work (Fig. 2(b-I)) [20]. Here, we identify the resonant peaks of our transducer at which it can deliver high acoustic power and compare it with that of the propeller response at these frequencies. Next, we experimentally characterize the rotational motion of both Type I and II propellers in the same range of acoustic frequencies (Fig. 2(b-II)). We observe that both the propellers show fast rotational motion at the resonant frequency (f_{res}) of 41 kHz. Although a few instances of the propellers also rotate at 55 kHz, their motion could be attributed to higher resonant harmonics as reported with other bubble-powered propellers [26]. We also observe a much wider spectral spread at 41 kHz that theoretically corresponds to a wide distribution of L_b=60–75μm. Further, the precise value of L_b is subjective to the different degrees of hydrophobicity in each cavity. These minor differences in L_b may introduce anisotropy in the streaming behavior of the propeller's constituent cavities. As L_b cannot be controlled within $<1\mu$m range, it maybe possible that some bubbles are closer to the resonant frequency than the others. Despite these possible deviations in our f_{res}, we consistently observe higher rotational speeds of the propellers at 41 kHz in its neighboring frequency range of 38–42 kHz in our subsequent experiments. Hence, we evaluate the performance of both Type I and II propellers at f_{res}=41 kHz for a range of power modulation.

3.2. Rotational performance for power modulation

We analyze the rotational speeds (RPM) for both the Type I and II propellers for a power modulation up to 200V_{pp} (peak-to-peak voltage). The Type I propellers show rotational motion around their geometric center in the same directional sense as the alignment of their cavities, as shown in Fig. 3(a) (Movie S2). On the other hand, the Type II propellers first align themselves with their long axis upright with respect to the substrate (Movie S1), and then rotate around a fixed pivotal point in space. In this upright position, the Type II propellers rotate in the direction of helicity of their constituent cavities (Fig. 2(c) *inset*). Additionally, it can be seen that the shaft of the Type II propeller itself inscribes a circular motion, as shown in Fig. 3(b) (Movie S3).

The rotational speeds of both Type I and II propeller monotonically increases with acoustic power as summarized in Fig. 3(c). Beyond 120V_{pp}, the speeds of Type II propeller increases at a much slower rate. In general, an increase in acoustic power beyond 180V_{pp} occasionally drifts the propellers away from their point of rotation (Movies S2 and S3). This observation can be attributed to significant bulk streaming in the microchannel due to its volumetric resonance and microstreaming caused by cavitation induced bubbles. Nonetheless, the highest speed achieved by Type I and II propeller is 250 RPM and 400 RPM, respectively, which is comparable to that of tethered microfluidic gears. Furthermore, Type II propellers can reach much higher speeds owing to proportionally higher number of cavities per turn as compared that of Type I.

3.2.1. Effect of varying propeller cavity size and alignment

Although Type II propellers can reach higher RPMs, the propeller axis itself inscribes a circular motion which changes with power and may vary across samples. This observation can be attributed to cavity size (L) being comparable to that of the propeller shaft (400 μm), which may cause undesirable tilting of the shaft. As a result, some instances of Type II propellers drift away from their point of rotation during the course of experiments with power modulation (Movie S3). With regards to potential design improvements, we designed and tested two variants of the Type II propeller each with cavity of size $L = 50\mu$m with an angular tilt (θ) of 90° (*i.e., our original design*) and 30° to the propeller axis. Here, we observe that the radius (R) of the circle the propeller shaft inscribes decreases (Fig. 4(a–c), Movie S3) as:

$$R_{L=100\mu m,\theta=90^o} > R_{L=50\mu m,\theta=90^o} > R_{L=50\mu m,\theta=30^o} \tag{2}$$

A comparison between the rotational speeds of all the Type II propellers is summarized in Fig. 4(d). Although the resonant frequency for Type $\mathrm{II}_{L=50\mu m}$ is higher than that of Type $\mathrm{II}_{L=100\mu m}$, we analyzed their speeds at 41 kHz for ease of comparison. Hence, we observe lower RPMs for Type $\mathrm{II}_{L=50\mu m}$ in contrast. Overall, we observe that Type $\mathrm{II}_{L=50\mu m,\theta=30^o}$ inscribe circular motion around its geometrical center akin to a screw.

3.2.2. Magneto-acoustic actuation

In addition to acoustically-induced rotation, we devise a hybrid actuation strategy where we combine magnetic steering and acoustic propulsion to achieve more targeted manipulation of these propellers. Here, we subject metallic Type I propellers, described earlier in Section 2.1, to magneto-acoustic actuation. We observe that the Type I propeller spontaneously aligns along one of the cavity axes when a constant and uniform magnetic field is applied. This axis can be either of the two opposite pairs of cavities that require a minimum restoring torque to align with the applied field direction (Movie S4). When magnetic field is

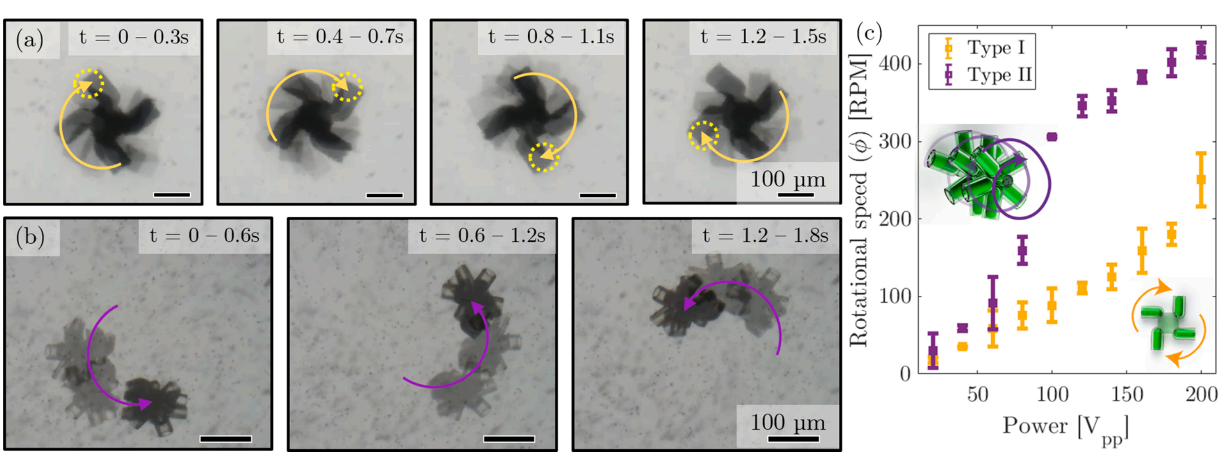

Fig. 3. Time-lapse image of a (a) Type I and (b) Type II propeller showing rotational motion. Each time-stamp comprises of super-imposed images of three successive positions of the propellers in the direction along the arrows, respectively. (c) Characterization of Type I and Type II propellers with a power modulation at resonance frequencies of 41kHz.

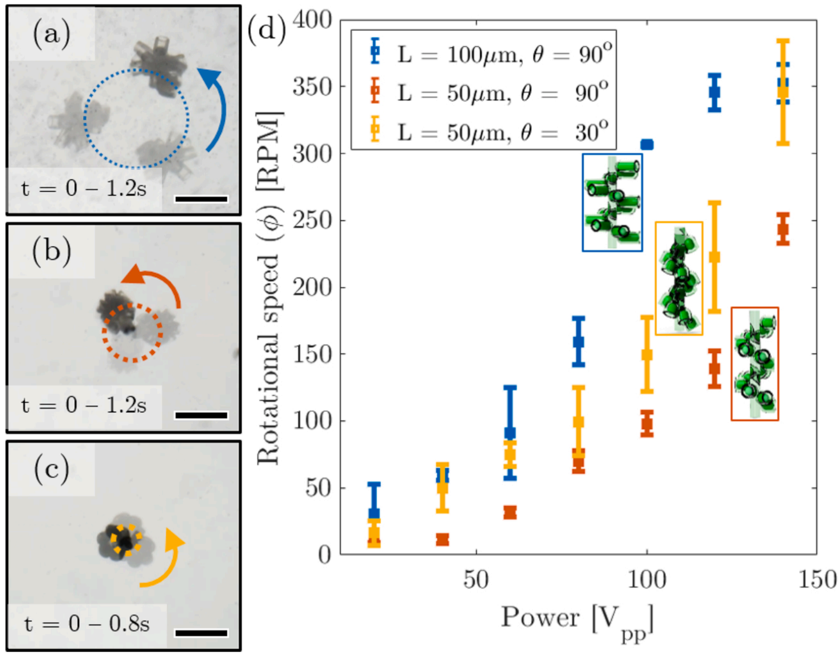

Fig. 4. (a–c) Time-lapse images of three different design variants (L,θ) of Type II propeller. The colored circles correspond to the respective color scheme depicted in the (d) legend. Each time-stamp comprises of super-imposed images of three successive positions of the propellers in the direction along the arrows, respectively. Scale bar represents 200μm. (d) Power modulation of the three Type II propeller variants at a frequency of 41kHz.

applied, a Type I propeller in rotation under acoustic field instantaneously locks in the direction of magnetic field and ceases to perform rotational motion. In this locked state, the dominant of the four cavities pushes the entire Type II propeller forwards along its direction. Theoretically, the propulsive forces due to the two opposite cavities should cancel out each other. However, we observe slight differences in the propulsive forces at the cavities owing to experimental factors such as unequal bubble lengths or magnitude of streaming (SPF). This heterogeneity in SPF due to the cavities is capitalized here to steer the propellers towards a desired target as they propel unidirectionally. Finally, when the magnetic field is switched off, the propeller resumes its rotational motion as depicted in Fig. 5(a). Since the unidirectional propulsion arises from the heterogeneous response of different cavities, this net directional force can be further pronounced at high acoustic powers. Hence, we test magneto-acoustic actuation at higher powers (>100V_{pp}) to ascertain effective unidirectional propulsion. Lastly, we demonstrate several cycles of acoustic rotation and magneto-acoustic steering in succession for increasing acoustic power, as shown in Fig. 5(b–d) (Movie S4).

4. Discussion

4.1. Conclusions

We present monolithic bubble-powered micro-propellers inspired from the design and functionality of gears. Our propellers address the present challenges of cost-effectiveness and resuability of conventional micromixers as they provide comparable rotational speeds while being untethered from any vibrating substrate. We explore two propeller designs which consist of an axis-symmetric distribution of bubble-entrapped cavities that are powered under acoustic actuation to provide streaming-induced rotational motion. Our Type-I propeller rotates akin to tethered microfluidic gears under acoustic actuation at speeds of up to 250 RPM. In addition, we present a hybrid actuation strategy to steer Type I propellers using magnetic fields. Hence, these propellers can be transported to different parts of the workspace to perform operations such as mixing solvents or targeted payload delivery. Next, we describe the Type II propellers which consist of a 3-D helical distribution of bubble-entrapped cavities that reach faster rotational speeds up to 400 RPM. The Type II propellers present an innovative concept to recreate existing 2-D mixers to attribute 3-D mixing ability throughout the volume of a fluid. Besides micro-mixing, the resultant bulk flow produced around these propeller can be exploited to provide local mechanical stimulation to cells seeded in microfluidic workspaces [35,36]

4.2. Future work

Both the Type I and II propellers can be redesigned with different cavity lengths tunable to different acoustic frequencies. Specifically, a distribution of two such cavity geometries in an oppositely arranged manner around the Type I propeller can facilitate their bidirectional rotation. Likewise, alternate Type II propellers with shorter cavities presented here could be investigated for screw-like motion. This screw-like motion of Type II propellers have the potential to exploit our magneto-acoustic actuation strategy to mimick the most popular magnetically-actuated helical microrobots [37]. Furthermore, improvements in magnetic deposition techniques can enable a more distinct alignment of our propellers in a desired orientation for a more controllable steering [18]. Moreover, SBF can be capitalized to explore interaction between multiple propellers whereby they can join forces with each other to enhance their efficacy such as higher mixing speeds. Further investigations with regards to the aforementioned design, fabrication improvements and cooperative behavior of these propellers can pave way for their biological and lab-on-a-chip applications.

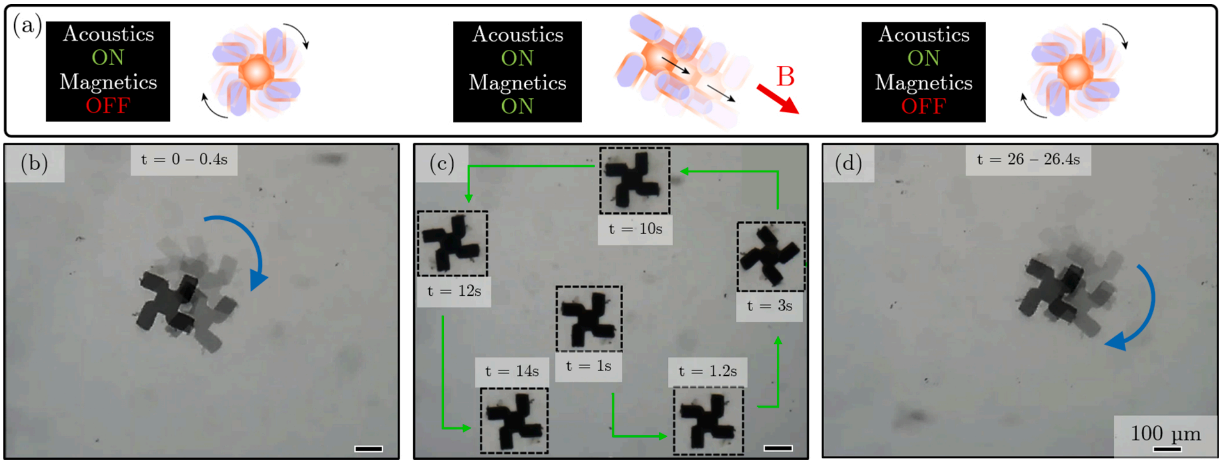

Fig. 5. Combined magneto-acoustic propulsion of Type I propeller: (a) Actuation scheme showing pure acoustic rotation followed by magneto-acoustic linear propulsion. Time-lapse sequence of Type I propeller as (b) it rotates under acoustic field (41kHz, *blue*), (c) steers and follows the trajectory under constant magnetic field (1mT, *green*), and (d) resumes rotational motion when magnetic field is turned off (Movie S4). Each time-stamp in (b) and (d) comprises of super-imposed images of four successive positions of the propellers in the direction along the arrows, respectively(For interpretation of the references to color in this figure legend, the reader is referred to the web version of this article.).

Author statement

Sumit Mohanty: Conceptualization, Methodology, Data curation, Writing – original draft.
Jiena Zhang: Methodology, Fabrication, Formal analysis.
Jeffrey M. McNeill: Methodology, Fabrication, Writing – review and editing.
Thom Kuenen: Software.
Frederic P. Linde: Simulations.
Jeroen Rouwkema: Supervision, Writing – review and editing.
Sarthak Misra: Conceptualization, Supervision, Funding acquisition, Writing – review and editing.

Conflicts of interest

None declared.

Declaration of Competing Interest

The authors report no declarations of interest.

Acknowledgements

We would like to thank Nick Helthuis for the assistance with SEM. We also thank Remco Sanders andMert Kaya for the assistance with experimental setup. We are grateful to Dr. Rory Dijkink for the insightful theoretical discussions throughout the preparation.

Appendix A. Supplementary data

Supplementary data associated with this article can be found, in the online version, at https://doi.org/10.1016/j.snb.2021.130589.

References

[1] V. Magdanz, I.S. Khalil, J. Simmchen, G.P. Furtado, S. Mohanty, J. Gebauer, H. Xu, A. Klingner, A. Aziz, M. Medina-Sánchez, O.G. Schmidt, S. Misra, IRONSperm: sperm-templated soft magnetic microrobots, Sci. Adv. 6 (28) (2020).
[2] D. Li, C. Liu, Y. Yang, L. Wang, Y. Shen, Micro-rocket robot with all-optic actuating and tracking in blood, Light Sci. Appl. 9 (1) (2020) 1–10.
[3] D. Ahmed, M. Lu, A. Nourhani, P.E. Lammert, Z. Stratton, H.S. Muddana, V. H. Crespi, T.J. Huang, Selectively manipulable acoustic-powered microswimmers, Sci. Rep. 5 (1) (2015) 1–8.
[4] L. Ren, D. Zhou, Z. Mao, P. Xu, T.J. Huang, T.E. Mallouk, Rheotaxis of bimetallic micromotors driven by chemical-acoustic hybrid power, ACS Nano 11 (10) (2017) 10591–10598.
[5] B.A. Darmawan, S.B. Lee, V.D. Nguyen, G. Go, K.T. Nguyen, H.S. Lee, M. Nan, A. Hong, C.S. Kim, H. Li, D. Bang, J.O. Park, E. Choi, Self-folded microrobot for active drug delivery and rapid ultrasound-triggered drug release, Sens. Actuators B. Chem. 324 (2020) 128752.
[6] P. Zhang, H. Bachman, A. Ozcelik, T.J. Huang, Acoustic microfluidics, Ann. Rev. Anal. Chem. 13 (2020) 17–43.
[7] S. Martel, O. Felfoul, J.B. Mathieu, A. Chanu, S. Tamaz, M. Mohammadi, M. Mankiewicz, N. Tabatabaei, MRI-based medical nanorobotic platform for the control of magnetic nanoparticles and flagellated bacteria for target interventions in human capillaries, Int. J. Robot. Res. 28 (9) (2009) 1169–1182.
[8] M.A. Ghanem, A.D. Maxwell, Y.N. Wang, B.W. Cunitz, V.A. Khokhlova, O. A. Sapozhnikov, M.R. Bailey, Noninvasive acoustic manipulation of objects in a living body, Proc. Natl. Acad. Sci. U. S. A. 117 (29) (2020) 16848–16855.
[9] S. Mohanty, Q. Jin, G.P. Furtado, A. Ghosh, G. Pahapale, I.S.M. Khalil, D. H. Gracias, S. Misra, Bidirectional propulsion of arc-shaped microswimmers driven by precessing magnetic fields, Adv. Intell. Syst. 2 (9) (2020) 2000064.
[10] Z. Yang, L. Zhang, Magnetic actuation systems for miniature robots: a review, Adv. Intell. Syst. 2 (9) (2020) 2000082.
[11] S.Y. Chin, Y.C. Poh, A.C. Kohler, J.T. Compton, L.L. Hsu, K.M. Lau, S. Kim, B. W. Lee, F.Y. Lee, S.K. Sia, Additive manufacturing of hydrogel-based materials for next-generation implantable medical devices, Sci. Robot. 2 (2) (2017) eaah6451.
[12] S. Mohanty, I.S.M. Khalil, S. Misra, Contactless acoustic micro/nano manipulation: a paradigm for next generation applications in life sciences, Proc. R Soc. A. Math. Phys. Eng. Sci. 476 (2243) (2020) 20200621.
[13] A.G. Guex, N.D. Marzio, D. Eglin, M. Alini, T. Serra, The waves that make the pattern: a review on acoustic manipulation in biomedical research, Mater. Today 10 (2021) 100110 [Online]. Available: https://doi.org/10.1016/j.mtbio.2021.100110.
[14] D. Petta, V. Basoli, D. Pellicciotta, R. Tognato, J. Barcik, C. Arrigoni, E.D. Bella, A. R. Armiento, C. Candrian, R.G. Richards, M. Alini, M. Moretti, D. Eglin, T. Serra, Sound-induced morphogenesis of multicellular systems for rapid orchestration of vascular networks, Biofabrication 13 (1) (2020) 015004.
[15] E.S. Comeau, D.C. Hocking, D. Dalecki, Ultrasound patterning technologies for studying vascular morphogenesis in 3D, J. Cell Sci. 130 (1) (2017) 232–242.
[16] J. Jeong, D. Jang, D. Kim, D. Lee, S.K. Chung, Acoustic bubble-based drug manipulation: Carrying, releasing and penetrating for targeted drug delivery using an electromagnetically actuated microrobot, Sens. Actuators A. Phys. 306 (2020) 111973.
[17] J. Park, J.y. Kim, S. Pané, B.J. Nelson, H. Choi, Acoustically mediated controlled drug release and targeted therapy with degradable 3D porous magnetic microrobots, Adv. Healthc. Mater. 10 (2) (2021) 2001096.
[18] L. Ren, N. Nama, J.M. McNeill, F. Soto, Z. Yan, W. Liu, W. Wang, J. Wang, T. E. Mallouk, 3D steerable, acoustically powered microswimmers for single-particle manipulation, Sci. Adv. 5 (10) (2019) eaax3084.
[19] R.J. Dijkink, J.P. Van Der Dennen, C.D. Ohl, A. Prosperetti, The 'acoustic scallop': a bubble-powered actuator, J. Micromech. Microeng. 16 (8) (2006) 1653.
[20] S. Mohanty, U. Siciliani de Cumis, M. Solsona, S. Misra, Bi-directional transportation of micro-agents induced by symmetry-broken acoustic streaming, AIP Adv. 9 (3) (2019) 035352.
[21] Y. Zhou, H. Wang, Z. Ma, J.K. Yang, Y. Ai, Acoustic vibration-induced actuation of multiple microrotors in microfluidics, Adv. Mater. Technol. 5 (9) (2020) 2000323.

[22] M. Kaynak, A. Ozcelik, N. Nama, A. Nourhani, P.E. Lammert, V.H. Crespi, T. J. Huang, Acoustofluidic actuation of in situ fabricated microrotors, Lab Chip 16 (18) (2016) 3532–3537.
[23] J. Li, M. Pumera, 3D printing of functional microrobots, Chem. Soc. Rev. 50 (4) (2021) 2794–2838.
[24] J.F. Louf, N. Bertin, B. Dollet, O. Stephan, P. Marmottant, hovering microswimmers exhibit ultrafast motion to navigate under acoustic forces, Adv. Mater. Interfaces 5 (16) (2018) 1800425.
[25] A. Aghakhani, O. Yasa, P. Wrede, M. Sitti, Acoustically powered surface-slipping mobile microrobots, Proc. Natl. Acad. Sci. U. S. A. 117 (7) (2020) 3469–3477.
[26] J.M. McNeill, N. Nama, J.M. Braxton, T.E. Mallouk, Wafer-scale fabrication of micro- to nanoscale bubble swimmers and their fast autonomous propulsion by ultrasound, ACS Nano 14 (6) (2020) 7520–7528.
[27] D. Ahmed, C. Dillinger, A. Hong, B.J. Nelson, Artificial acousto-magnetic soft microswimmers, Adv. Mater. Technol. 2 (7) (2017) 1700050.
[28] Q. Chen, F.W. Liu, Z. Xiao, N. Sharma, S.K. Cho, K. Kim, Ultrasound tracking of the acoustically actuated microswimmer, IEEE Trans. Biomed. Eng. 66 (11) (2019) 3231–3237.
[29] J. Feng, J. Yuan, S.K. Cho, 2-D steering and propelling of acoustic bubble-powered microswimmers, Lab Chip 16 (12) (2016) 2317–2325.
[30] F.W. Liu, S.K. Cho, 3-D swimming microdrone powered by acoustic bubbles, Lab Chip 21 (2) (2021) 355–364.
[31] D. Jang, J. Jeon, S.K. Chung, Acoustic bubble-powered miniature rotor for wireless energy harvesting in a liquid medium, Sens. Actuators A. Phys. 276 (2018) 296–303.
[32] Y. Zhou, Z. Ma, Y. Ai, Submicron Particle concentration and patterning with ultralow frequency acoustic vibration, Anal. Chem. 92 (19) (2020) 12795–12800.
[33] S. Uran, M. Malok, B. Bratina, R. Šafarič, A pot-like vibrational microfluidic rotational motor, Micromachines 12 (2) (2021) 177.
[34] M. Kaynak, P. Dirix, M.S. Sakar, addressable acoustic actuation of 3D printed soft robotic microsystems, Adv. Sci. 7 (20) (2020) 2001120.
[35] Y. Guyot, B. Smeets, T. Odenthal, R. Subramani, F.P. Luyten, H. Ramon, I. Papantoniou, L. Geris, Immersed boundary models for quantifying flow-induced mechanical stimuli on stem cells seeded on 3d scaffolds in perfusion bioreactors, PLOS Comput. Biol. 12 (9) (2016 9) e1005108 [Online]. Available: https://journals.plos.org/ploscompbiol/article?id=10.1371/journal.pcbi.1005108.
[36] W. Yu, H. Qu, G. Hu, Q. Zhang, K. Song, H. Guan, T. Liu, J. Qin, A microfluidic-based multi-shear device for investigating the effects of low fluid-induced stresses on osteoblasts, PLOS ONE 9 (2) (2014 2) e89966 [Online]. Available: https://journals.plos.org/plosone/article?id=10.1371/journal.pone.008996.
[37] F. Qiu, B.J. Nelson, Magnetic helical micro- and nanorobots: toward their biomedical applications, Engineering 1 (1) (2015) 021–026.

Sumit Mohanty received a Bachelor's Degree in Instrumentation Engineering at IIT Kharagpur, India, and a Master's Degree in Nanotechnology at KTH Royal Institute of Technology, Sweden. Prior to his graduation, he was a visiting student at ETH Zurich, where he worked on magnetic actuation of micro-robots. He is currently pursuing his Doctoral degree in the Surgical Robotics Laboratory, Department of Biomechanical Engineering at University of Twente, The Netherlands. His doctoral research is focused on design, fabrication and actuation of magnetic and acoustic micro-robots.

Jiena Zhang received a Bachelorin Bioengineering at Hainan University, China,and a Master's Degree in Bioengineering at the University of Nottingham, UK. She is currently pursuing her Doctoral degree in the Vascularization Lab, Department of Biomechanical Engineering at the University of Twente, The Netherlands. Her doctoral research is focused on engineering perfusable and vascularized tissues.

Jeffrey M. McNiell received a Bachelor's Degree in Chemistry with a minor in Physics at the West Virginia Wesleyan College, USA. He is currently pursuing his Doctoral degree in the Mallouk group, Department of Chemistry at the University of Pennsylvania, USA. His doctoral research is focused on active matter, developing microsystems powered by acoustics and catalysis.

Thom Kuenen received a Bachelor's Degree in Biomedical Engineering from University of Twente, The Netherlands. He is currently pursuing a Master's Degree in Biomedical Engineering at the University of Twente, The Netherlands.

Frederic P. Linde received a Bachelor's Degree in Advanced Technology from University of Twente, The Netherlands. He is currently pursuing a Master's Degree in Robotics and Mechatronics at the University of Twente, the Netherlands. He is a part of the Surgical Robotics Laboratory, Department of Biomechanical Engineering at University of Twente, The Netherlands.

Jeroen Rouwkema received a Master's Degree in Process Engineering from Wageningen University, The Netherlands, and a Doctoral Degree in Tissue Engineering from the University of Twente, The Netherlands. He is currently an Associate Professor in the Department of Biomechanical Engineering, University of Twente, The Netherlands. His research interests include tissue engineering, microfluidics and 3D bioprinting, with the main focus on vascularization. He was the recipient of the European Research Council Consolidator and Proof-of-Concept Grants and the Netherlands Organization for Scientific Research VENI Grant.

Sarthak Misra received a Master's Degree in Mechanical Engineering from McGill University, Canada, and a Doctoral Degree in Mechanical Engineering from The Johns Hopkins University, USA. He is currently a Full Professor in the Department of Biomechanical Engineering, University of Twente, The Netherlands. He is also affiliated with the Department of Biomedical Engineering, University of Groningen, and University Medical Center Groningen, The Netherlands. Prior to commencing his doctoral studies, he was a Dynamics and Controls Analyst in the International Space Station Program. His research interests include surgical robotics and medical microrobotics. Prof. Misra was the recipient of the European Research Council Starting, Proof-of-Concept, and Consolidator Grants and the Netherlands Organization for Scientific Research VENI and VIDI Awards. He is a Co-Chair of the Robotics and Automation Society Technical Committee on Surgical Robotics and a Co-Chair of the International Federation of Automatic Control Technical Committee on Biological and Medical Systems.